Evaluation of hydrogen-Induced cracking resistance of the In625 laser coating system on a C-Mn steel substrate

http://dx.doi.org/10.1590/0370-44672016700088

Vicente Braz Trindade
Professor
Universidade Federal de Ouro Preto – UFOP
Escola de Minas
Departamento de Engenharia Metalúrgica
Ouro Preto – Minas Gerais - Brasil
vicentebraz@yahoo.com.br

Natália Chaves Almeida
Mestre pelo Programa de Pós-Graduação da REDEMAT - Rede Temática em Engenharia de Materiais da Universidade Federal de Ouro Preto
Ouro Preto – Minas Gerais - Brasil
nataliachavesalmeida@gmail.com

Luiz Cláudio Cândido
Professor Associado
Universidade Federal de Ouro Preto – UFOP
Escola de Minas
Departamento de Engenharia Metalúrgica
Ouro Preto – Minas Gerais - Brasil
candido@em.ufop.br

Geraldo Lúcio de Faria
Professor Adjunto
Universidade Federal de Ouro Preto – UFOP
Escola de Minas
Departamento de Engenharia Metalúrgica
Ouro Preto – Minas Gerais - Brasil
geraldolfaria@yahoo.com.br

Milton Sergio Fernandes de Lima
Professor do Programa de Pós-Graduação da REDEMAT - Rede Temática em Engenharia de Materiais da Universidade Federal de Ouro Preto
miltonsflima@gmail.com

Abstract

The corrosion of C-Mn steels in the presence of hydrogen sulfide (H_2S) represents a significant challenge to oil production and natural gas treatment facilities. The failure mechanism induced by hydrogen-induced cracking (HIC) in a Inconel 625 coating / C-Mn steel has not been extensively investigated in the past. In the present work, an API 5CT steel was coated with In625 alloy using laser cladding and the HIC resistance of different regions, such as the coating surface, the substrate and HAZ, were evaluated. SEM observations illustrated that all HIC cracks were formed at the hard HAZ after 96h of exposure. No HIC cracks were observed in the substrate and the In625 coating after the same exposure duration. Pitting was recorded in the substrate caused by non-metallic inclusion dissolving.

Keywords: Inconel 625, laser cladding, C-Mn steel API5CT, HIC resistance, pitting.

1. Introduction

In the petroleum industry, the application of piping is mandatory in many parts of the project for the production of oil and gas (upstream) as well as for transportation and refining (downstream). The materials commonly used to produce those pipes are C-Mn steels. However, for parts of the project C-Mn steels have not been complying with the project requirements, mainly regarding corrosion due to H_2S, which can cause catastrophic structural failure. The complete mechanism of failure by hydrogen-induced cracking (HIC) is not yet fully understood since it is a complex phenomenon depending on several aspects such as: microstructural characteristics, material composition, non-metallic incusion (composition, size and morphology) as well as mechanical loading and enviromental conditions, among others

(Carneiro *et al.*, 2003; Kittel *et al.*, 2010; Liang *et al.*, 2009; Solheim *et al.*, 2013; Wang *et al.*, 2013). When hydrogen atoms enter the material lattice, they diffuse to internal interfaces such as grain boundaries and non-metallic inclusions and recombine forming hydrogen molecule gas building up high local pressure. This can originate HIC cracks depending on the material microstructure toughness. Increased yield stress is known to increase the accumulation of hydrogen in the crack tip where a maximum triaxial tensile stress is present (Yokobori *et al.*, 2002; Krom *et al.* 1999).

Therefore, more noble materials are required, such as austenitic steels and/or Ni-based superalloys. However, the manufacturing of the entire pipe body using these noble materials can sharply affect the cost, since these materials are very expensive when compared to C-Mn steels. A technological solution is to develop appropriate coatings using these noble materials on the surface of C-Mn steel pipes (Abioyea *et al.*, 2015).

The objective of this study is to evaluate the HIC susceptibility of the system In625 laser coating/steel substrate, including the heat affected zone (HAZ) formed due to the thermal cycle imposed to the steel substrate during laser welding.

2. Materials and methods

The material used for this study is a seamless steel pipe grade API5CT, with outside diameter = 244.5 mm and wall thickness = 13.84 mm, hot rolled followed by quenching & tempering heat treatment. The chemical composition is shown in Table 1.

C	Mn	Mo	Ni	Si	Ti	Al	Cr	B
0.25	1.05	0.06	0.10	0.20	0.030	0.025	0.35	0.0016

Table 1
Chemical composition (wt.%) of the steel used (Fe is the balance).

The laser depositing was performed using a longitudinal speed of 240mm/min and laser power of 10kW and the focal length of the lens was 136mm. Figure 1 shows an exemple of an as-deposited coupon. The inconel 625 deposition was in average 0.107 g/mm^2.

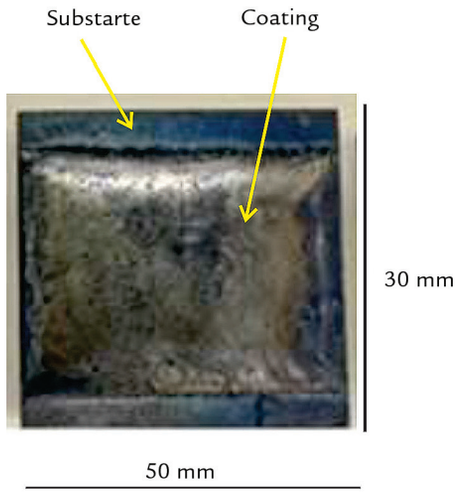

Figure 1
As-deposited laser coupon showing the dimensions of the samples.

The chemical composition of the used Inconel 625 is given in Table 2.

Cr	Mo	Nb	Al	Ti	Fe	Mn	Si	C	Co
22.0	9.0	3.6	0.4	0.4	2.5	0.4	0.3	0.1	0.9

Table 2
Chemical composition (wt.%) of the Inconel 625 used (Ni is the balance).

Microstructural characterizations were performed using light microscope and scanning electron microscope (SEM) integrated with energy-dispersive X-ray spectroscopy (EDX). Transversal cuts were made in order to investigate the cross section of the coating and interface coating/substrate (steel). The specimens were prepared by grinding with 1200 mesh SiC paper and polished with diamond paste of 1 µm and 0.5 µm size. Etching in Nital 2% was used to observe the substrate microstructure and electrolytic etching (current of 2 A and voltage of 10V) with a solution of 10 vol.% of oxalic acid ($C_2H_2O_4.2H_2O$) was used to observe the coating microstructure.

Vickers hardness measurement was done in order to evaluate the hardness

profile along the cross section of the coating/substrate. The load was 1 kgf and the procedure is according to the ASTM E384-99 standard.

Specimens of100 mm length by 20 mm width specimens with three different thicknesses were used in order to evaluate the coating surface exposed to corrosive environment, the HAZ exposed to corrosive environment, and the as-received base metal exposed to corrosion environment as shown in Figure 2. The specimen surfaces to be analyzed were finely ground with 1000-mesh SiC-paper prior to corrosion exposure.

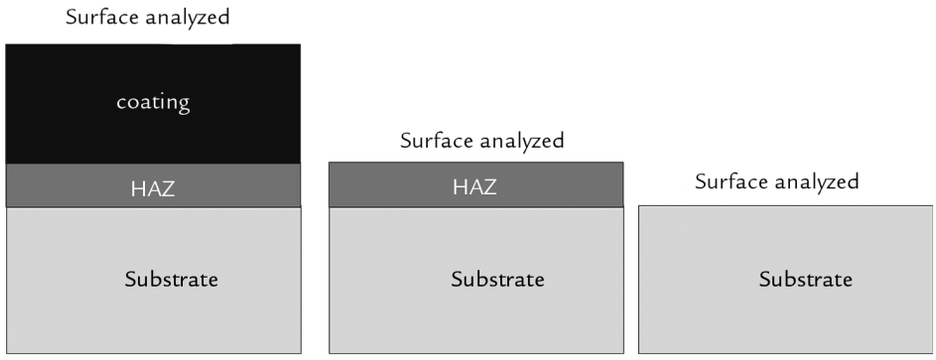

Figure 2
Schematic representation of the specimens used for corrosion analysis. The HAZ analyzed surface is below the dilution zone.

The corrosive solution used was according to TM0284-96 standard, solution A, which consists of 50.0g of NaCl and 5.00g of CH_3COOH dissolved in 945g of distilled water. The initial pH measured was 3. The nitrogen purge gas and H_2S were injected near the botton of the test vessel. As soon as the specimens were put in the test vessel in the solution, the vessel was sealed and purged using nitrogen for 2h at a rate of 100cm^3/h. After purging, H_2S was bubbling into the sealed vessel at a constant flow rate in such a way that the measured concentration of H_2S using iodometric titration was 3,500 ppm at the end of the test. The temperature was kept between 24°C and 26°C. The test lasted 96h in the described condition.

After exposure, the specimens were cleaned to remove scales and deposits. The surface was analyzed using scanning electron microscopy.

3. Results and discussion

Microhardness measurement along the cross section of the deposited coating, prior to corrosion, is shown in Figure 3. As we can see, the coating presented a microhardness that was not too differente from the microhardness of the substrate. On the other hand, a peak of microhardness (417HV1) was observed in the heat affected zone (HAZ).

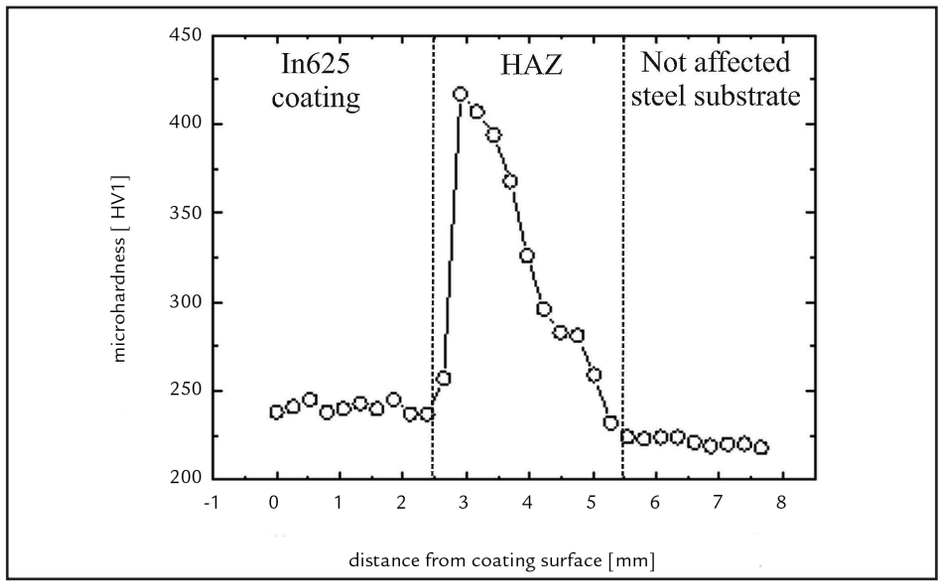

Figure 3
Microhardness profile of the coating/substrate cross section.

The microstructure of the substrate (steel) observed by using SEM analysis after the Nital 2% etching is as expected, that means, tempered martensite, as shown in Figure 4a. In the area of the microhardness peak (HAZ), the original microstructure of the substrate is destroyed during the thermal cyle imposed by the laser depositing process. The final microstructure reveals to be a lower bainite structure as shown in Figure 4b and supported by literature (Abbaszadeh *et al.*, 2012), demonstrating that this hardness is in the magnitude range of lower bainite. On the other hand, the martensite hardness level would be around 700HV for a similar C-Mn steel. The microstructure of the coating is similar to those classical as-cast microstructures during welding. Figure 4c shows the columnar grains in dendritic morphology with carbides (mainly Mo and Nb carbides –white phases) within the interdendritic spaces. The thickness of the coating was on average 2.5mm. Figure 4d shows the composition profile of the main elements, showing an abrut change on Fe, Cr and Ni on metal/substrate interface.

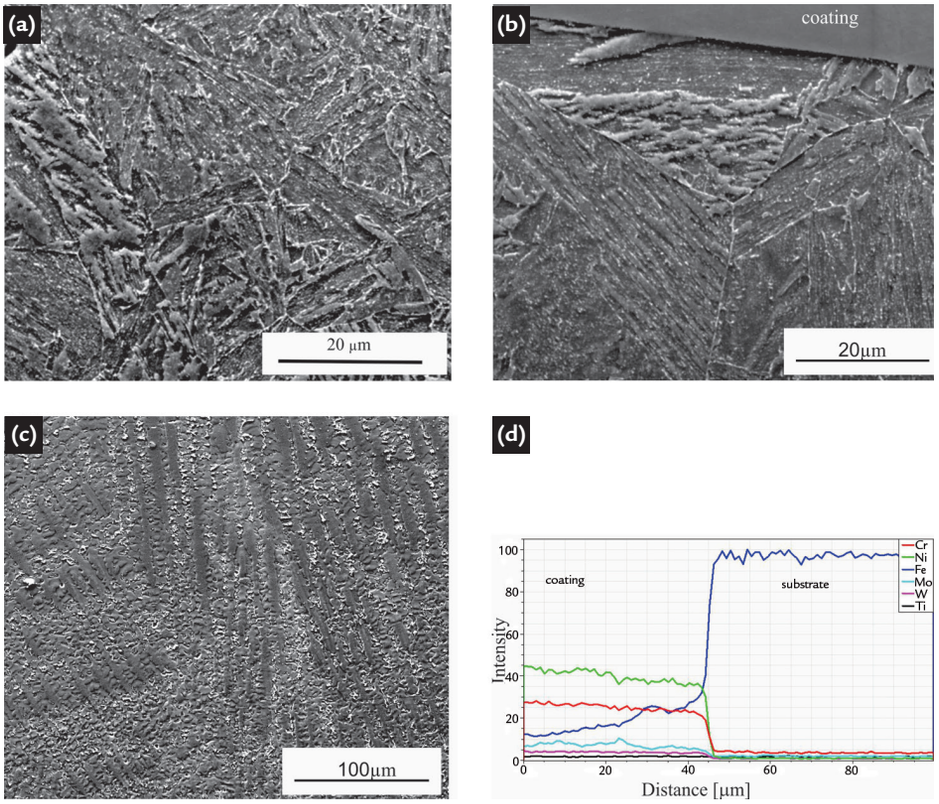

Figure 4
Microstructure prior to corrosion: (a) base metal is not affected by thermal gradient, (b) HAZ, (c) In625 coating and (d) EDS measured chemical profile of main elements.

The cross section of the coating in Figure 5a shows a micro view of the substrate/coating. Figure 5b shows a higher magnification of the interface substrate/coating pointing out the presence of a large dilution zone of around 30µm of thickness, which shall be decreased by choosing better laser deposition parameters. The element chemical profiles across the dilution layer is shown in Figure 5c, where the Fe diluted into the coating. This dilution zone was not exposed to the HIC test.

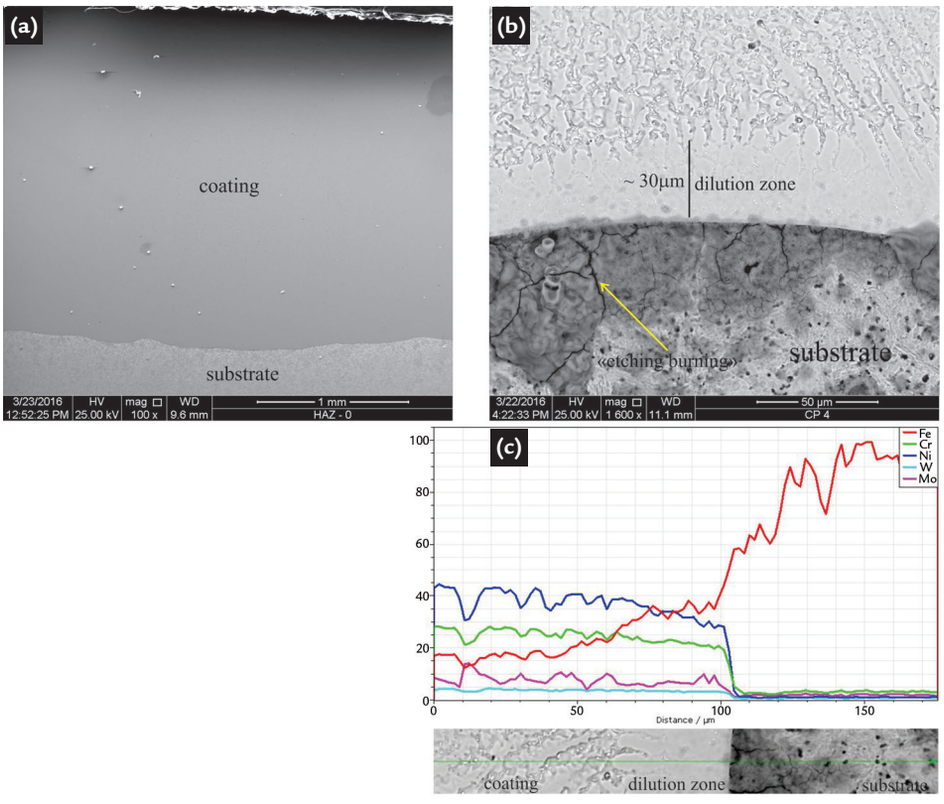

Figure 5
Cross section of coating.
(a) macro view, (b) dilution zone and (c) the EDS element profiles along the dilution zone.

After exposure (96h) to corrosion, no corrosion attack (cracking and pitting) was observed on the coating surface as shown in Figure 6a. For the specimen, which has the original substrate surface exposed to corrosive environment, no cracking was observed, but some pits were observed as shown in Figure 6b. This attack can be attributed to the inclusion dissolved by the corroding solution.

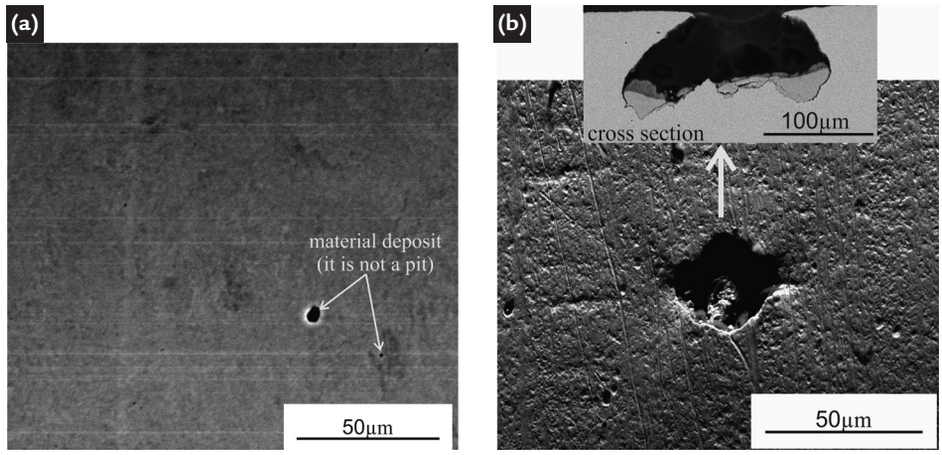

Figure 6
Surface analysis after corrosion exposure: (a) In625 coating and (b) substrate.

The substrate presented inclusion of a different chemical nature, especially those of mixed oxide based on Al, Ca and Mg, as well as a mixture of sulphide as shown in Figure 7. It has been demonstrated in literature (Lang *et al*, 2015) that these kinds of inclusions are soluble when exposed to a corroding media such as Solution A as per TM0284-96 standard.

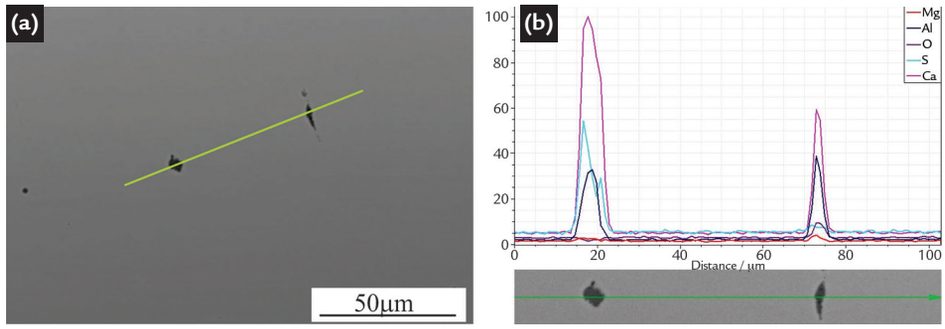

Figure 7
Inclusion analysis observed in the substrate. (a) SEM picture and (b) EDS analysis.

However, when exposing the surface of the HAZ to the corrosive environment, a severe corrosion attack was observed (Figure 8). This observation leads us to the conclusion that bainite has a deleterious effect to the resistance to hydrogen-induced cracking.

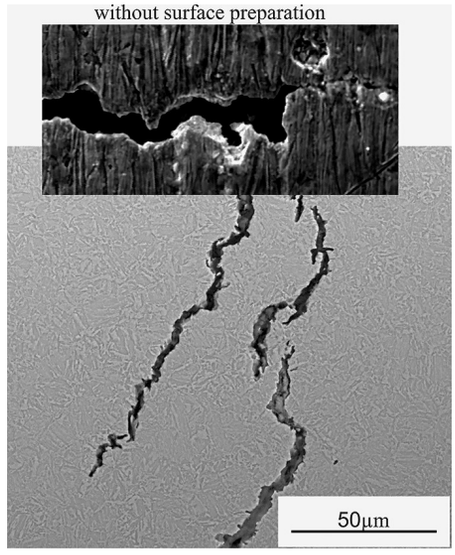

Figure 8
Surface analysis after corrosion exposure of the HAZ.

The crack sentivity ratio (CSR), crack length ratio (CLR) and crack thickness ratio (CTR) were calculated according to NACE TM0284 standard. Table 3 shows the HAZ higher sentivity to the hydrogen-induced cracking phenomenon.

Table 3
Calculated crack sentivity ratio (CSR), crack length ratio (CLR) and crack thickness ratio (CTR).

Region	CSR (%)	CLR (%)	CTR (%)
Substrate	0	0	0
HAZ	1.4	32	3.1
Coating	0	0	0

This study demonstrates the efficiency of an In625 coating to protect steel structures, e.g. pipes, against hydrogen-induced cracking. Furthermore, if the coating is mechanically damaged or if it is not thick enough, hydrogen can reach the HAZ causing massive cracking, which can lead to failure of the whole system.

It is reported in literature that there is a beneficial effect of bainite to the hydrogen-induced cracking resistance (Carneiro *et al*., 2013) when working with low carbon steel with less than 0.1wt.% of carbon. However, in this present study, a medium carbon steel (C=0.25wt.%) was used combined with different conditions for the bainite formation compared to the thermomechanical processed steel studied by Carneiro et al., resulting in different morphologies of the bainite. In the present work, the needle-like lower bainite seems to be deleterious to the hydrogen-induced cracking.

Furthermore, due to the complexity of the hydrogen-induced cracking phenomenon, more probable other parameters can influence such as residual stress, segregation, specimen preparation, among others.

4. Conclusions

The present study allows the drawing of the following conclusions:

(1) Laser cladding causes a hard HAZ at the coating/substrate interface of C-Mn API5CT steel.

(2) The In625 coating deposited by laser welding on API5CT steel reveals to be an excellent protection of C-Mn steel against HIC, since no cracking and no pitting was observed after exposure to corrosion in Solution A according to NACE TM0284 standard.

(3) Although, the substrate demonstrated to have good HIC resistance, pitting was observed caused by non-metallic inclusion dissolution in the corrosive medium.

(4) When exposing the HAZ to the corrosive environment, the HIC phenomenon happens acutely forming several cracks on the surface. This seems to be due to the high hardness of this region, which is formed by needle-like lower bainite phase.

Acknowledgments

This research has been supported by the Brazilian Research Foundation (CAPES) through a fellowship to one of the authors (Natália Chaves Almeida).

References

ABBASZADEH, K., SAGHAFIAN, H., KHEIRANDISH, S. Effect of bainite morphology on mechanical properties of the mixed bainite-martensite microstructure in D6AC steel. J. ***Mater. Sci. Technol.***, v. 28, p. 336-342, 2012.

ABIOYEA T.E., MCCARTNEY D.G., CLAREA A.T. Laser cladding of Inconel 625 wire for corrosion protection. ***Journal of Materials Processing Technology,*** v. 217, p. 232–240, 2015.

CARNEIRO, R.A., RATNAPULI R.C., LINS V.F.C. The influence of chemical composition and microstructure of API, linepipe steels on hydrogen induced cracking and sulfide stress corrosion cracking. ***Mater. Sci. Eng. A***, v. 357, p. 104–110, 2003.

KITTEL J., SMANIO V., FREGONESE M., GARNIER L., LEFEBVRE X. Hydrogen induced cracking (HIC) testing of low alloy steel in sour environment: impact of time of exposure on the extent of damage. ***Corros. Sci.***, v. 52, p. 1386–1392, 2010.

KROM A. H. M., KOERS R. W. J., BAKKER A. Hydrogen transport near a blunting crack tip. ***J. Mech. Phys. Solids,*** v. 47, p. 971-992, 1999.

LANG F.J., HUANG X.Q., PANG T., MA Y., CHENG P., HE R. Effect of inclusion on pitting corrosion of X80 pipeline steel. ***Advance Materials Research,*** v.1120-1121, p.999-1002, 2015.

LIANG P., DU C.W., LI X.G. Effect of hydrogen on the stress corrosion cracking behavior of X80 pipeline steel in Kuerle Soil Simulated Solution. ***Int. J. Miner. Metall. Mater.,*** v. 16, p. 407–413, 2009.

SOLHEIM K.G., SOLBERG J.K. Hydrogen-induced stress cracking in supermartensitic stainless steels-stress threshold for coarse grained HAZ. ***Eng Fail Anal.***, v. 32, p. 348-355, 2013.

WANG L.W., DU C.W., LIU Z.Y., WANG X.H., Li X.G. Influence of carbon on stress corrosion cracking of high strength pipeline steel. ***Corros Sci.,*** v. 7, p. 486-495, 2013.

YOKOBORI A.T., CHINDA JR., Y., NEMOTO T., SATO K., YAMADA T. The characteristics of hydrogen diffusion and concentration around a crack tip concerned with hydrogen embrittlement. ***Corro Sci,*** v. 44, p. 407-424, 2002.

Received: 9 June 2016 - Accepted: 11 November 2016.